

Structure and Deformations of Pd–Ni Core–Shell Nanoparticles

S. Sao-Joao,[†] S. Giorgio,^{*,†} J. M. Penisson,[§] C. Chapon,[†] S. Bourgeois,[‡] and C. Henry[†]

CRMCN-CNRS, Campus de Luminy, Case 913, 13288 Marseille Cédex 9, France, UMR5613 CNRS/Université de Bourgogne, UFR Sciences et Techniques, BP 47870 Dijon Cédex, France, and DRFM/SP2M/ME Bat C5, 435, CEA-G, 17 Rue des Martyrs, 38054 Grenoble Cédex 9, France

Received: June 30, 2004

Homogeneous collections of Pd–Ni core–shell nanoparticles have been prepared by decomposition of metal–organic compounds and studied by several electron microscopy techniques: transmission electron microscopy (TEM), energy-dispersive X-ray spectroscopy (EDS), high-resolution transmission electron microscopy (HRTEM), energy-filtered microscopy (EFTEM), and by X-ray photoelectron spectroscopy (XPS). The physical and chemical properties of the Pd shell are supposed to depend on its electronic properties, which are influenced by the presence of the Ni core and by the deformation in the Pd lattice. Here, the interfacial structure of Pd/Ni and the lattice deformations in the core and the shell are studied in detail. The catalytic properties of the pure metal and the bimetallic particles, toward CO oxidation, have been investigated.

1. Introduction

Bimetallic particles with the core–shell structure represent a new class of materials to improve or tune the catalytic activity or selectivity of catalytic reactions. The tuning of the catalytic properties is connected to the variation of the electronic structure of the surface atoms which are influenced by core and shell atoms.^{1–5} Indeed, at the particle surface, the heteronuclear metal–metal bonds induce a shift of the valence band center in the first monolayers. Aside from this effect, variations in the coordination number of the surface atoms and strains also move the valence band center. In a core–shell cluster, the outside layer can be different from the bulk structure because of the influence of the core and also its small size. A very large number of publications exists in the domain of core–shell clusters from colloid solutions. We have already prepared Pd–Cu core–shell clusters.⁶

The reactivity of surfaces of Pd–Ni systems has been investigated toward the hydrogenation of butadiene, in the case of the (110) surface of the Pd₈Ni₉₂(110) alloy⁷ and in the case of thin Pd layers deposited on a Ni(110) surface.^{8,9} Four monolayers of Pd have been found to be 40 times more active than a Pd(110) single crystal, which shows the highest activity for this reaction.

From a comparison between these studies and *ab initio* calculations,⁵ it was concluded that the catalytic properties of the Pd–Ni bimetallic system is related both to the changes in the electronic properties and in the atomic structure. Complex structures were evidenced. In extended Ni/Pd interfaces, periodic vacancies are produced from the stress induced by Ni.¹⁰

The morphology and structure at the interface of Ni particles or thin Ni layers supported on MgO have been studied by grazing incidence X-ray scattering.¹¹

In this paper, we elaborate on Pd–Ni core–shell particles in epitaxy on MgO microcrystals, by decomposition of Pd and Ni acetyl acetonates (acac). The lattice deformations at the

interfaces Pd/Ni and Ni/MgO are investigated by HRTEM and the coexistence of Ni²⁺/Ni by XPS. The activity of these particles toward CO oxidation has been studied as well as that of pure Pd and Ni clusters.

2. Preparation Techniques, Composition of Pd–Ni Particles

Pure Ni particles were prepared by the decomposition of Ni(acac)₂ on MgO oxide powders, then the Pd shells were grown on the Ni particle surfaces from solution, following the previously described techniques.^{11,12} The Ni(acac)₂ (Fluka, 40–90 mg) was dissolved in acetonitrile (200 mL). MgO clean powders (Fluka, 200 mg) with a surface specific area of 30 m² g⁻¹ were mixed into the solution and stirred at 80 °C until complete evaporation of the solvent. After drying at 80 °C in air, the powders were slowly annealed in a vacuum (10⁻⁴ Torr), until 450 °C, then reduced under H₂ at 400 Torr during 3 h at the same temperature. At this stage, the core was prepared. Different amounts (8–50 mg) of Pd(acac)₂ (Aldrich) were dissolved in toluene (200 mL). The oxide powders with Ni particles on their surfaces were mixed with the solution and heated under a flux of bubbling H₂ until complete evaporation of the solvent. In the solution at high temperature (until 119 °C) and with H₂, the decomposition of Pd(acac)₂ occurs, and then, the Pd atoms directly crystallize on the Ni clusters. If the temperature is too low, and without H₂ in solution, the decomposition of Pd(acac)₂ does not occur, and then, the compound is directly adsorbed on MgO, and Pd crystallizes separately from Ni. Then, the samples were annealed once again in a vacuum (10⁻⁴ Torr) until 450 °C before alloy formation.

The particles were analyzed by EDS in an electron microscope (JEOL 2000 FX). Their composition was determined either on isolated clusters in convergent beam mode or on collections of clusters in standard analysis. For structural studies, other microscopes were used (JEOL 4000EX and JEOL 3010).

The experimental Ni loading in Ni/MgO clusters, measured by EDS, is plotted in Figure 1 as a function of the mass of Ni(acac)₂ for 200 mg of clean MgO. If we compare the experimental Ni loading to the ratio of Ni over MgO mass concentration in the solution, we conclude that about one-half

* Corresponding author.

[†] CRMCN-CNRS, Campus de Luminy. Associated to Universities of Aix-Marseille 2 and 3.

[‡] UMR5613 CNRS/Université de Bourgogne.

[§] DRFM/SP2M/ME Bat C5.

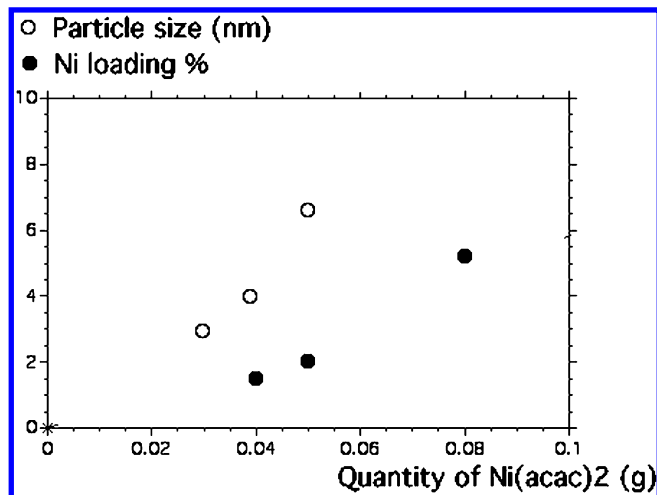


Figure 1. (●) Ni loading in weight in the sample, according to the quantity of Ni(acac)₂ in solution. (○) Ni particle size.

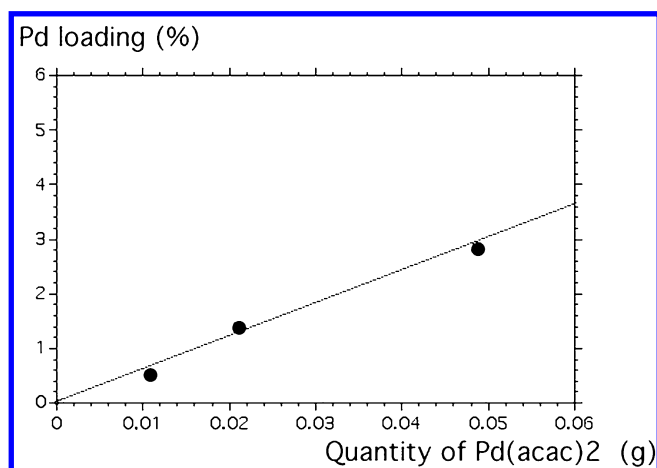


Figure 2. Pd loading in weight in the Pd/Ni/MgO sample, according to the quantity of Ni(acac)₂ in solution. The data were obtained from Ni/MgO samples with a loading of 3% by weight.

of the Ni is lost during the impregnation (we noticed that a colored deposit is visible on the glass vessel).

The atomic concentration of Pd in the core–shell particles directly increases with the quantity of Pd(acac)₂ in the solution. As seen in Figure 2 for a Ni/MgO with 3% of Ni, the Pd loading in the Pd/Ni/MgO sample is roughly proportional to the Pd(acac)₂ concentration in the solution. Interestingly, this allows control of the thickness of the shell.

3. Particle Size, Morphology, Composition, and Crystalline Structures

All of the samples were observed in TEM, either by EFTEM (with a JEOL 3010 equipped with a Gatan imaging filter) or in HRTEM (with a JEOL 4000EX, $C_s = 0.5$ mm, and a JEOL 3010, $C_s = 0.6$ mm).

The size of the pure Ni particles grows with the Ni (acac)₂ concentration in solution, as seen on Figure 1. For quantities higher than 0.06 g of Ni(acac)₂ for 200 mg of MgO in the standard preparation, the size distribution of the particles becomes much broader than for smaller depositions.

Figure 3 is an HRTEM image of a pure Ni particle of about 3 nm in size, (001) epitaxially oriented on MgO, limited by 4 (111) faces and truncated at the top by a (001) face. The ratio between the height and the diameter is $h/D = 0.4$. The shape is close to the equilibrium shape found in the case of Pd particles

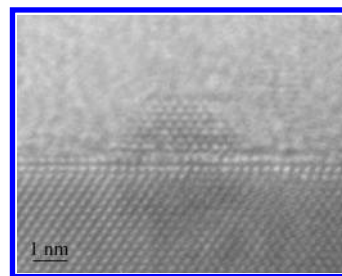


Figure 3. Small Ni particle limited by 4 (111) faces, seen in profile view along [110].

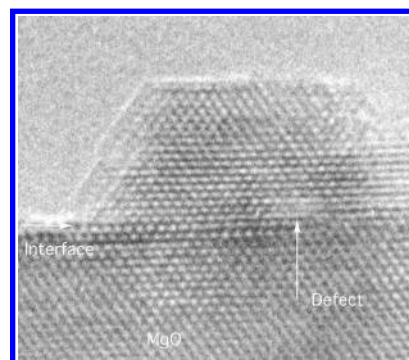


Figure 4. Ni particle limited by 4 (111) faces and truncated at the top by a (001) face. The limited number of defects at the interface despite a large misfit (17%) is certainly due to NiO formation in the first metal layers.

of the same size.¹³ Here, the Ni lattice is completely accommodated to the MgO substrate and dilated by 17%. The distances between the atomic columns were measured along the directions parallel to the interface, with the MgO taken as an internal calibration. The lattice of Ni is completely accommodated to the lattice of MgO, at least in the first six layers from the interface. For larger particle sizes (Figure 4), the shape is a top-truncated half-octahedron; few local defects are seen at the interface. The ratio between the height and the diameter is $h/D = 0.7$, which is larger than in the case of small Ni particles.

If the particle has the equilibrium shape, the aspect ratio is related to the adhesion energy between the deposit and the substrate.

For equivalent sizes, the observed Ni particles on MgO are more truncated at the interface than the Pd particles.¹⁴ Moreover, with σ_{100} Ni being larger than σ_{100} Pd,^{14,15} one expects from the Wulff Kaishev theorem less truncations for Ni particles.

In the Ni/MgO samples, by XPS, both Ni⁰ and Ni^{II} are clearly detected.

The good accommodation of the metal to the substrate is certainly due both to deformations and to the partial formation of oxide, near the interface. Indeed, the outside lateral surfaces of the particles are of (111) type, and the equilibrium morphology of NiO particles of any size corresponds to cubes, just limited by (100) faces at all the edges. During the observation in the microscope, the pure Ni particles are transformed in NiO despite the reducing effect of the electrons. In Figure 5a,b,c,d, a series of images of the same 4-nm-sized particle are taken with intervals of irradiation doses of about 2×10^4 C m⁻².

In Figure 5a, the particle limited by (111) faces starts to be truncated at the edges and the top by (100) faces. As in the previous cases, a dislocation can be seen at the interface at the right side, due to the misfit with MgO. The aspect ratio h/D is about 0.57, but it is not clear at all if the particles still have the equilibrium shape. For an oxide (NiO), the conditions to get the equilibrium are certainly more demanding (very high

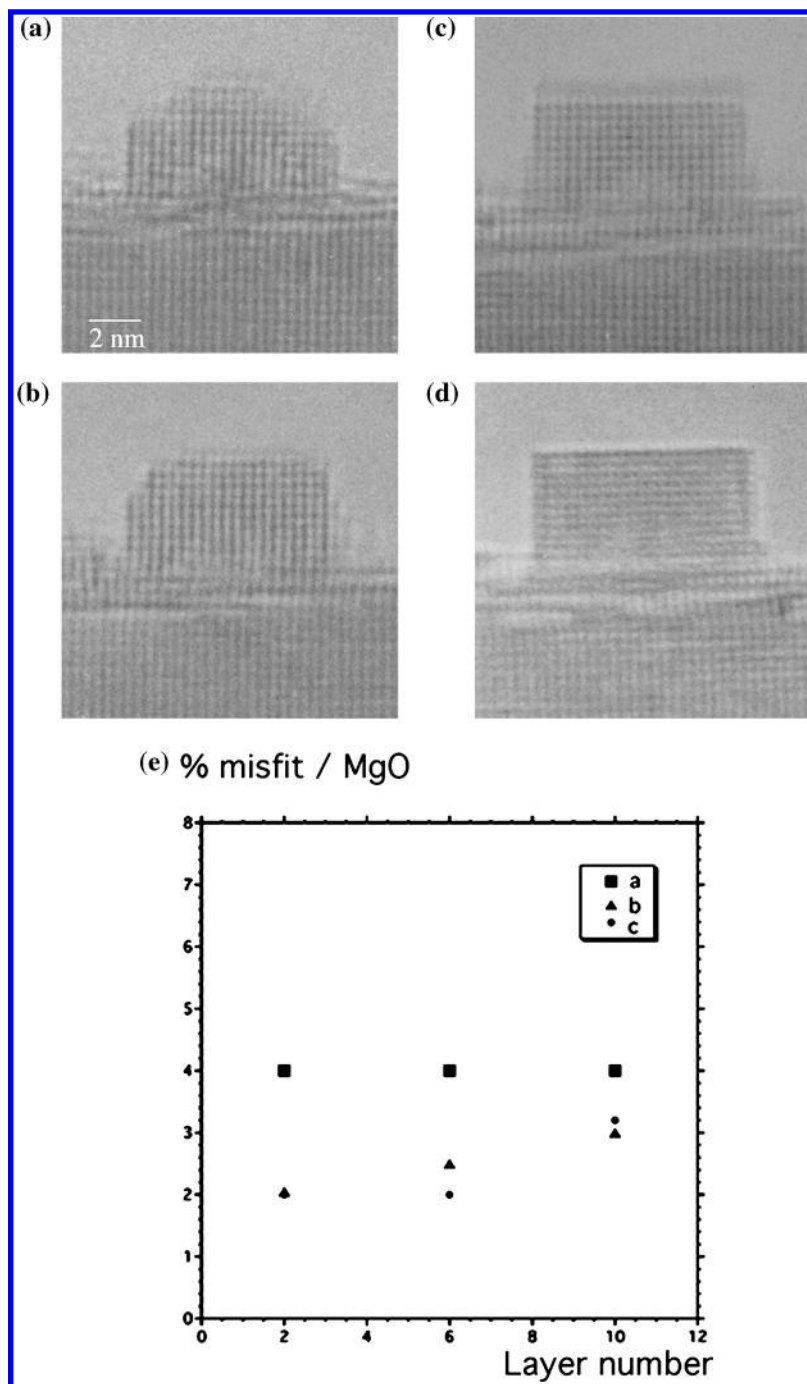


Figure 5. (a, b, c, d) Evolution of a Ni particle during the observation in the electron beam. (e) Evolution of the misfit between the particle and MgO near the interface, in the volume and near the top of the particles (a, b, c).

temperature) than for metals. In Figure 5b, the shape is mainly limited by (100) faces, the dislocation still exists exactly at the middle part of the interface, and the aspect ratio is higher than in the preceding case. Then, in Figure 5c, the shape is only limited by (100) faces with sharp edges, and the interface is quasiperfect without dislocations. After that step, the shape no longer evolves (Figure 5d), and the interface stays perfect.

The distance between the (200) lattice fringes in the particles, perpendicular to the interface, are measured by numerical analysis and compared to the spacing in MgO taken as the internal calibration. The misfit between bulk Ni and MgO is high, 17%.

The results are reported in Figure 5e. In (a), the (200) distances in the cluster are dilated, but the misfit with MgO is about 4% in all of the volume. In the same particle (b) after an

irradiation of $2 \times 10^4 \text{ C m}^{-2}$, the lattice is more expanded, but the misfit still exists with MgO, by 2% near the interface and more than 3% in the volume. After the same irradiation doses (c), the 2% misfit remains the same near the interface and in the volume. The shape of the particle is that expected for a NiO particle only exposing (100) facets. However, the lattice of the particle is still contracted relative to bulk NiO. The misfit between NiO and MgO is 0.7%. A possible explanation could be that the particle is not stoichiometric.

The transformation from Ni to NiO is clearly a microscope artifact, and this is the evidence that as soon as the clusters are limited by (111) faces, they are not yet transformed in NiO in the volume, even if NiO starts to grow near the interface.

It can be observed that pure NiO in an electron microscope can be easily reduced in Ni,¹⁶ but in our case, the Ni clusters

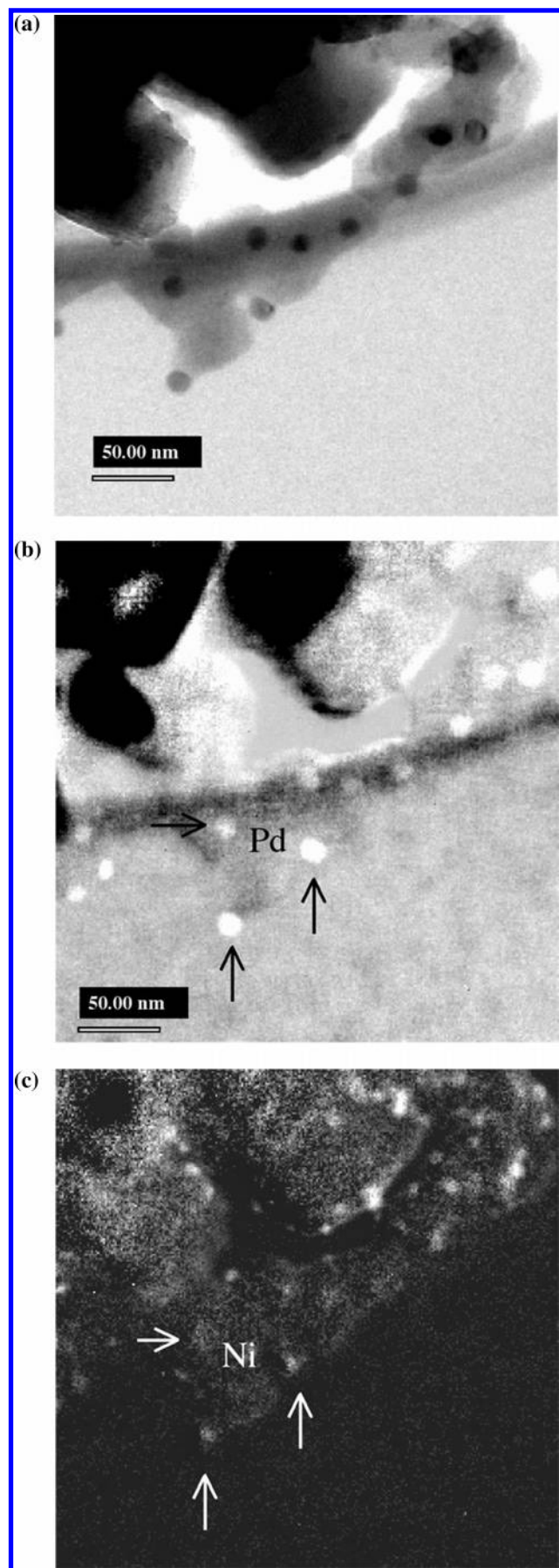


Figure 6. (a) Bright field image of Pd/Ni core–shell particles. (b) Energy-filtered image with the peak Pd M 45 at 335 eV. (c) Energy-filtered image with the peak Ni L3 at 855 eV.

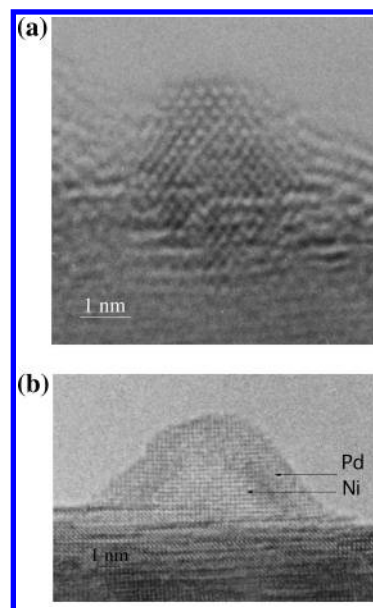


Figure 7. (a) Small Pd–Ni particle seen in profile view along a [110] direction. (b) Large Pd–Ni core–shell particle seen in profile view along a [100] direction.

are epitaxially oriented on MgO and more influenced by the substrate. We believe that the oxidation of Ni starts at the Ni–MgO interface in order to minimize the interfacial energy.

The Pd/Ni core–shell particles are homogeneous in composition. The energy-filtered images (Figure 6) are able to show the Ni core, from the peak L3, at 855 eV (Figure 6c) and the Pd shell, from the peak M 45, at 335 eV (Figure 6b) in each cluster seen in Figure 6a. The particle sizes in Figure 6a,b are equal, and the particle sizes in Figure 6c are smaller. It can be deduced that all of the large clusters are bimetallic. However, some very small Ni clusters can be detected on the surface. According to the XPS analysis of these samples, the Ni is found as Ni⁰ and Ni^{II}.

The general morphology and crystalline structure of the Pd–Ni core–shell particle looks like the particles seen in Figure 7a,b.

Figure 7a shows a small Pd/Ni particle of about 3 nm. The Pd shell is made of 5 layers. The particle is seen in a [110] direction, parallel to the (111) lateral faces. The difference of contrast between the center and the shell is low, because of the small particle size, but the resolution in the image is improved in the external parts which do not contain Ni in the projection. Below the interface, some high-resolution fringes are seen in the MgO with a strong contrast, which can be due to local deformations in the substrate. Such deformations in MgO were never observed in previous studies of Pd/MgO, but in these cases, the misfits were weak (8% with Pd).

Figure 7b is a larger particle with a Pd shell made of about 10 layers. The Ni core is perfectly oriented (001) on MgO. The Pd shell is epitaxially oriented on the core. Despite the particle size, no dislocations are visible at the interface Ni/MgO. The quasiperfect accommodation at the interface is once again interpreted by the partial oxidation of Ni interface atoms.

Slight deviations of the (200) fringes normal to the interface of metal/oxide are seen at the interface of Pd/Ni. However, these deformations are too weak to be measured quantitatively by numerical analysis of the HRTEM images, by the technique of the intensity profiles.¹⁷ The lattice deformations were investigated from the phase images of Figure 8a by using the geometric phase method.¹⁸

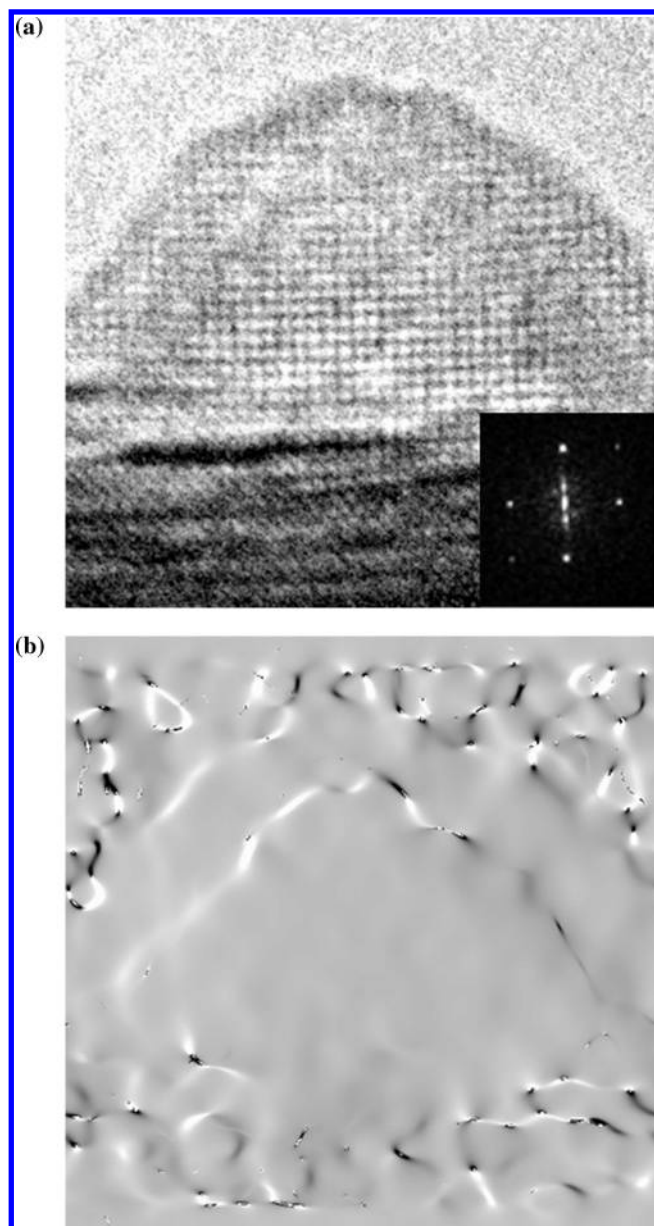


Figure 8. (a, b) Pd–Ni core–shell particle (a) with the Power spectrum, displacement along the [100] direction (b).

If the reciprocal lattice vector in the image of the shell differs from the reference lattice vector (\mathbf{g}) of the core by $\Delta\mathbf{g}$, then the phase can be written as a function of the position: $P\mathbf{g}(r) = 2\pi\Delta\mathbf{g}r$.

The displacement field $u(r)$ is determined by combining two sets of lattice fringes (200) and (020), shown in the power spectrum (in Figure 8a) of the square image (Figure 8a). The vectors \mathbf{a}_1 and \mathbf{a}_2 represent the lattice in the real space, in the [100] and [010] directions, and then the displacement vector is

$$u(r) = -(1/2\pi)[P\mathbf{g}_1(r)\mathbf{a}_1 + P\mathbf{g}_2(r)\mathbf{a}_2]$$

The displacement field is clearly visible near the Pd/Ni interface in Figure 8b where the phase image changes. However, the displacement field at the level of Ni/MgO does not follow the interface. Thus, we conclude that the Pd layer in the shell is locally strained without dislocations and that the Ni–MgO interface is not homogeneously distorted. The critical thickness corresponding to the formation of misfit dislocations in a continuous Pd layer, in epitaxy on Ni, can be estimated by a

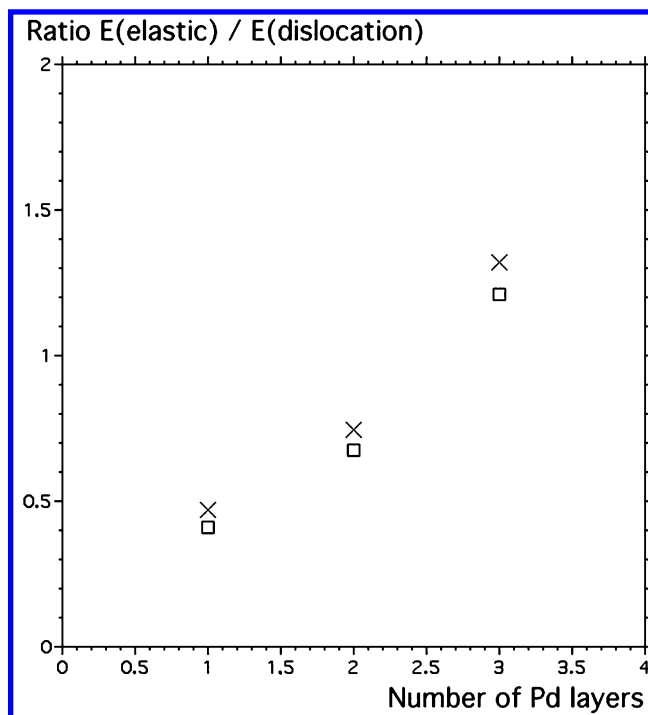


Figure 9. Plot of the calculated ratio between the elastic energy and the energy of dislocation, according to the number of Pd layers crystallized on bulk Ni. $E_{el}/E = 2 \cdot (1 + \nu_{\text{mét}}/1 - \nu_{\text{mét}})\delta_2 \cdot h / [(Ln(h/b\perp) + 1)/2\pi(1 - \nu_{\text{mét}})]$, with $\nu_{\text{mét}}$ = Poisson coefficient of Pd ($\nu_{\text{mét}} = 0.39$), δ_2 = misfit between Pd and Ni, $b\perp$ = Burgers vector = $(1/2)$ at Pd-[100] or $(1/2)$ [110], according to the direction of dislocations, and h = thickness of the Pd layer.

simple calculation of the ratio between the elastic energy and the energy of dislocations in Pd.¹⁹ The ratio between the elastic energy and the energy of dislocations (E_{el}/E_{disl}) can be calculated.

Dislocations are formed when $E_{el}/E_{\text{disl}} > 1$. For increasing thicknesses between 1 and 3 nm, similar to the thickness of the Pd layer in Figure 7, this ratio is calculated and plotted in Figure 9 for both directions of dislocations [100] and [110]. It can be seen that below 2.7 nm, which is similar to the thickness of the Pd layers in the shells, in both directions, the elastic energy is lower than the energy of dislocations, and then the system is thermodynamically more stable with deformations instead of dislocations.

4. Catalytic Test

The catalytic activity of these preparations has been tested on the oxidation of CO.

The sample of MgO powders covered with the Pd/Ni, Pd, or Ni particles is introduced at room temperature in a quartz closed reactor (130 cm³). After evacuation down to 10⁻⁶ mbar, CO and O₂ were introduced at the same partial pressure of 2 mbar. The reactor is linearly heated, and the gas composition in the reactor is continuously recorded by sampling the gas through a leak valve connected to a UHV chamber equipped with a quadrupole mass spectrometer. The leak valve is regulated to maintain a pressure of 1 × 10⁻⁸ mbar in the vacuum chamber. The total pressure inside the reactor is continuously recorded by a capacitance manometer.

In Figure 10, the evolution of the reaction rate for CO₂ production is plotted as a function of time in three cases. The estimated temperature inside the reactor is indicated along the time axis. Three samples were tested, each containing the same atomic amount of metal, for a total loading of 7% in weight in

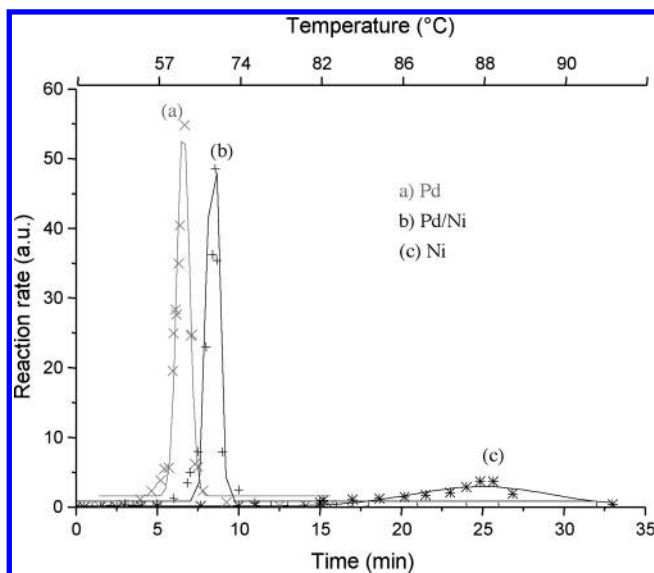


Figure 10. Rate of CO₂ production in the reactor, as a function of the time, during heating from room temperature to 100 °C.

TABLE 1: Reaction Rate at 50% Conversion and Maximum Reaction Temperature for Each Sample, for Two Cycles of Reaction

	Ni/MgO		Pd/Ni/MgO		Pd/MgO
	1	2	1	2	
reaction rate at 50% conversion (Torr/min)	0.07			0.24	0.31
maximum reaction rate temperature (°C)	88			70	63

the catalyst. Sample **a** contains 100% of Pd atoms, **b** 15% of Pd and 85% of Ni, and **c** 100% of Ni.

The respective quantities used for the elaboration of each sample are given. Sample **a** was elaborated with 150 mg of MgO and 39.28 mg of Pd(acac)₂. Sample **b** was elaborated with 150 mg of MgO, 5.55 mg of Pd(acac)₂, and 28.3 mg of Ni(acac)₂. Sample **c** was elaborated with 150 mg of MgO and 32.9 mg of Ni(acac)₂.

It is clearly seen that **a** and **b** catalysts present similar behaviors for the oxidation of CO, while **c** is poorly active and only at higher temperature. Table 1 clearly shows that deactivation does not occur in the Pd–Ni catalyst. So, it is clear that the core–shell structure is stable during the catalytic reaction and does not alloy in the particles.

As the reactivities of pure Pd and Pd–Ni particles are very close, it is evident that the use of core–shell clusters with Pd outside allows us to save important amounts of Pd.

5. Discussion

The chemical structure and geometrical deformations in Ni–Pd core–shell particles supported on MgO have been ex situ studied by XPS and various techniques of TEM.

XPS indicates the partial oxidation of the Ni in the particles. This oxidized Ni is at least due to the air transfer, but the partial oxidation of Ni atoms at the Ni/MgO interface is another possible explanation.

After air transfer, bimetallic Ni₅₀Pt₅₀ catalysts and pure Ni supported on SiO₂²⁰ show the existence of NiO as observed by HRTEM.

In the case of Pd/Ni nanoparticles, the coexistence of Ni and NiO in the core allows a perfect lattice accommodation with MgO (001) in the “cube-on-cube orientation”. The NiO formation at the interface of Ni/MgO can be explained by the ability of Pd to dissociate O₂, then by the diffusion of atomic oxygen through the shell.

The outer shape of pure Ni particles observed on MgO(001) is typical from better wetting than for Pd/MgO, which is unexpected for pure Ni. The corresponding increase of the adhesion energy is also explained by the existence of interfacial NiO that decreases the misfit with MgO.

The adhesion energy calculated²¹ for various transition metals on Mg and on O indicates a weak interaction which normally leads to a more isotropic shape, with reentrance angles at the interface. So, it seems reasonable to believe that NiO exists at the interface, which increases the adhesion energy of the cluster.

For the average size (5–7 nm) of our core–shell clusters, the catalytic activities toward CO oxidation are similar to the case of pure Pd clusters. As Pd is on the external faces, it represents an interesting savings of expensive metal. However, we do not observe an enhancement of reactivity for the core–shell clusters for the oxidation of CO, in contradiction with the experiments on four monolayers (ML) of Pd on Ni(110) in the case of butadiene hydrogenation.^{7,8} It is interesting to note that for this reaction, no increase of reactivity was observed on PdNi alloy particles,²² although the bulk alloys show an increase of reactivity. It has been recently shown that the enhancement of catalytic activity was due to a local strain in the Pd top layer in the case of four ML of Pd on Ni(110).¹⁰ A possible explanation for the absence of enhanced activity of small particles could be the presence of edges. By HRTEM, it is impossible to quantify the deformations on the first external layer.

References and Notes

- Rodriguez, J. A.; Goodman, D. W. *Science* **1992**, *257*, 897.
- Hammer, B.; Norskov, J. K. *Adv. Catal.* **2000**, *45*, 1.
- Holmblad, M.; Larsen, J. H.; Chorkendorff, I.; Pleth Nielsen, L.; Besenbacher, F.; Stensgaard, I.; Laegsgaard, E.; Kratzer, P.; Hammer, B.; Norskov, J. K. *Catal. Lett.* **1996**, *40*, 131.
- Ruban, A.; Hammer, B.; Stoltze, P.; Skriver, H. L.; Norskov, J. K. *J. Mol. Catal. A: Chem.* **1997**, *115*, 421.
- Filhol, J. S.; Simon, D.; Sautet, P. *Phys. Rev. B* **2001**, *64*, 85412.
- Giorgio, S.; Henry, C. R. *Eur. Phys. J. Appl. Phys.* **2002**, *20*, 23.
- Michel, A. C.; Lianos, L.; Rousset, J. L.; Delichère, P.; Prakash, N. S.; Massardier, J.; Jugnet, Y.; Bertolini, J. C. *Surf. Sci.* **1998**, *416*, 288.
- Hermann, P.; Guigner, J. M.; Tardy, B.; Jugnet, Y.; Simon, D.; Bertolini, J. C. *J. Catal.* **1996**, *163*, 169.
- Porte, L.; Phaner-Goutorbe, M.; Guigner, J. M.; Bertolini, J. C. *Surf. Sci.* **1999**, *424*, 262.
- Filhol, J. S.; Saint-Lager, M. C.; De-Santis, M.; Dolle, P.; Simon, D.; Baudoing-Savois, R.; Bertolini, J. C.; Sautet, P. *Phys. Rev. Lett.* **2002**, *14*, 8914.
- Barbier, A.; Renaud, G.; Robach, O. *J. Appl. Phys.* **1998**, *84*, 4259.
- Giorgio, S.; Chapon, C.; Henry, C. R. *Langmuir* **1997**, *13*, 2279.
- Graoui, H.; Giorgio, S.; Henry, C. R. *Philos. Mag. B* **2001**, *81*, 1649.
- Tyson, W. R.; Miller, W. A. *Surf. Sci.* **1977**, *62*, 267.
- Aldén, M.; Skriver, H. L.; Mirbt, S.; Johansson, B. *Surf. Sci.* **1994**, *315*, 157.
- Aronin, A.; Abrosimova, G.; Bredikhin, S.; Matsuda, K.; Maeda, K.; Awano, M. *J. Ceram. Soc. Jpn.* **2002**, *110* (8), 722.
- Giorgio, S.; Chapon, C.; Henry, C. R.; Nihoul, G. *Philos. Mag. B* **1993**, *67*, 773.
- Hytch, M. J.; Snoeck, E.; Kilaas, R. *Ultramicroscopy* **1998**, *74*, 131.
- Matthews, J. W.; Jackson, D. C.; Chambers, A. *Thin Solid Films* **1975**, *74*, 129.
- Rellinghaus, B.; Stappert, S.; Wassermann, E. F.; Sauer, H.; Spliethoff, B. *Eur. Phys. J. D* **2001**, *16*, 249.
- Goniakowski, J.; Noguera, C. *Interface Science* **2004**, *12*, 93.
- Renouprez, A.; Faudon, J. F.; Massardier, J.; Rousset, J. L.; Delichère, P.; Bergeret, G. *J. Catal.* **1997**, *170*, 181.